Three-dimensional magnetic-flux-closure patterns in mesoscopic Fe islands

R. Hertel,[1,*] O. Fruchart,[2] S. Cherifi,[2] P.-O. Jubert,[3] S. Heun,[4] A. Locatelli,[5] and J. Kirschner[6]
[1]*Institute of Solid State Research (IFF), Research Center Jülich, D-52425 Jülich, Germany*
[2]*Laboratoire Louis Néel, CNRS-UJF-INPG, BP166, F-38042 Grenoble Cedex 9, France*
[3]*IBM Research, Zurich Research Laboratory, CH-8803 Rüschlikon, Switzerland*
[4]*TASC-INFM Laboratory, Area di Ricerca, Basovizza, I-34012 Trieste (TS), Italy*
[5]*Sincrotrone ELETTRA, I-34012 Basovizza, Trieste, Italy*
[6]*Max-Planck Institute of Microstructure Physics, Weinberg 2, 06120 Halle, Germany*
(Received 23 June 2005; revised manuscript received 6 September 2005; published 6 December 2005)

We have investigated three-dimensional magnetization structures in numerous mesoscopic Fe/Mo(110) islands by means of x-ray magnetic circular dichroism combined with photoemission electron microscopy (XMCD-PEEM). The particles are epitaxial islands with an elongated hexagonal shape with length of up to 2.5 μm and thickness of up to 250 nm. The XMCD-PEEM studies reveal asymmetric magnetization distributions at the surface of these particles. Micromagnetic simulations are in excellent agreement with the observed magnetic structures and provide information on the internal structure of the magnetization which is not accessible in the experiment. It is shown that the magnetization is influenced mostly by the particle size and thickness rather than by the details of its shape. Hence these hexagonal samples can be regarded as model systems for the study of the magnetization in thick, mesoscopic ferromagnets.

DOI: 10.1103/PhysRevB.72.214409 PACS number(s): 75.60.Ch, 75.75.+a, 75.40.Cx, 79.60.−i

I. INTRODUCTION

The spatial confinement of the magnetization in a ferromagnet of mesoscopic or nanometric size can have a dramatic impact on both the magnetic properties and the magnetization distribution.[1–5] Besides the technological importance of understanding and controlling such finite-size effects in magnetic nanoparticles that can be used for magnetoelectronic devices, the physics of the magnetization in confined structures is a beautiful and exciting research topic.[54] A precise theoretical description of the magnetization distribution in particles of a size between about 100 nm and a few microns can be obtained in the framework of micromagnetism.[6,7] Generally, the micromagnetic equations can only be solved numerically. Mesoscopic magnetic particles are too small for a meaningful description in terms of macroscopic material constants like the magnetic susceptibility. On the other hand, the simple macrospin model—which could be solved analytically[8]—can only be applied for very small ($\lesssim$10 nm) magnetic particles.[9] It loses its validity in larger ferromagnets, where the magnetization distribution is strongly inhomogeneous.

The subtle size dependence of the magnetization[10–12] is particularly important when the particle size is comparable to the so-called magnetic exchange length,[5,13] i.e., a material-dependent length scale that describes the order of magnitude for the extension of magnetic inhomogeneities like domain walls or magnetic vortices. Besides the size, also the particle shape is known to have a strong influence on the magnetic properties of nanostructures. Numerous studies on magnetic particles of different geometries, like rings,[14] rectangles,[4] nanowires,[15] and various other geometries[2,16,17] have been reported in the past years. Apart from a few exceptions where three-dimensional magnetic structures have been investigated numerically (e.g., Refs. 18–20), experimentally[21] or both,[22] most studies on magnetic nanostructures that have been published over the last years have focused on particles in which *at least one* dimension is so small that the magnetization in the sample is either two-dimensional (thin-film elements) or one-dimensional (thin nanowires). Therefore, compared to thin film elements, where the influence of the particle shape on the magnetic properties has been amply studied, not much is known about the effect of spatial confinement in three-dimensional magnetic particles.

Similarly, several types of magnetic domain walls[23–26] have been investigated thoroughly in extended magnetic films.[5] In these studies, the sample was essentially confined in one dimension (the film thickness). Recently, the influence of geometric confinement on domain walls has been studied in systems with two-dimensional[27] and one-dimensional[28] magnetization, and different types of head-to-head domain walls have been predicted[29] and observed[30] in thin magnetic strips or rings of different width. However, the effect of a mesoscopic spatial confinement of *three-dimensional* magnetic domain walls has hardly been investigated up to now.

In this paper we report on three-dimensional magnetization distributions in mesoscopic ferromagnets. As a model system, we have analyzed several monocrystalline Fe islands of different size (up to ca. 2.5 μm length and up to ca. 250 nm thickness). These particles are small enough to display pronounced finite-size effects of the magnetization, while they are sufficiently large and thick to sustain inhomogeneous, three-dimensional arrangements of the magnetization. The experimental part of this study is performed by means of x-ray magnetic circular dichroism with photoemission electron microscopy (XMCD-PEEM). The direct comparison of high-resolution experimental observations with highly accurate micromagnetic computer simulations allows for an unambiguous interpretation of some complicated, unexpected magnetization distributions. This analysis leads us to the conclusion that the Landau pattern, which is well

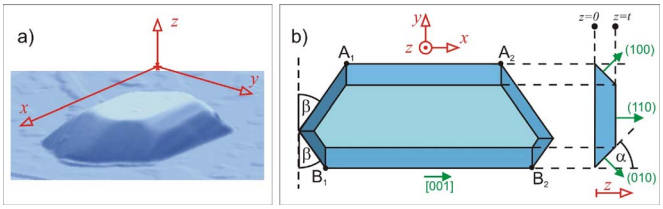

FIG. 1. (Color online) (a) Atomic force microscopy of a Fe island, about 1 μm long. (b) Schematic presentation of a typical particle geometry. The angles α=45° and β=35.26° are fixed parameters that result from the monocrystalline structure of the islands. The shape is uniquely defined by the points A_1, A_2, B_1, B_2 and the thickness t. Note that this set of parameters is subject to various constraints. For instance, the edges (A_1,A_2) and (B_1,B_2) are parallel to each other (the x direction).

known from magnetic thin-film elements, is merely a simple variant of a general, more complex magnetization structure.

II. SAMPLE PREPARATION

Mesoscopic monocrystalline Fe islands have been grown on atomically flat Mo(110) buffer layers of thickness 10 nm,[31] deposited on $Al_2O_3(11\bar{2}0)$. The growth is performed with pulsed laser deposition (PLD) in ultrahigh vacuum at 850 K. Under these conditions, Fe islands are formed by means of the Stranski-Krastanov growth mode. A cover layer of Mo[three atomic layers], followed by Al[3 nm] has been added to protect the samples from oxidation. A more detailed description of the fabrication of self-assembled Fe/Mo(110) islands is reported elsewhere.[32,33] The islands have a hexagonal shape, a flat top and inclined lateral facets, all atomically flat; see Fig. 1(a).

If the growth proceeded under thermodynamic equilibrium, the shape of all islands would be expected to be identical, and described by the Wulff-Kaischev theorem (see Ref. 34 and references therein). We indeed observe that the islands share a common set of features: the angle of inclination of the lateral facets, the horizontal top facet, as well as the direction of all edges. However, the shape of the particles is generally not symmetric and not uniform. The vertical and in-plane aspect ratios slightly differ from one to another. This may arise from kinetic effects, the influence of atomic steps on the Mo(110) surface or residual strain. The size ranges between about 500 nm to 2500 nm in length and about 50 to 250 nm in thickness. Our observations suggest that the shape of the particles is well reproduced by taking into account only {001} and {110} facets. The examination of the constraints related to these facets leads to an idealized geometrical construction scheme for the shape of these islands as described in Fig. 1. Using this scheme, each island is uniquely described by the four points A_1,A_2,B_1,B_2 and the thickness t. Approximate values for the thickness and the coordinates of these four points have been extracted from electron microscopy images to construct models that were used as input for the numerical simulations. The density of the islands on the substrate is low enough, so that generally speaking, the magnetostatic coupling between the samples is negligible. Obviously, a few exceptional cases can also be found, where two islands have formed in close vicinity.

These self-assembled Fe islands can be regarded as a model system for the study of magnetization distributions in three-dimensional, mesoscopic particles. Due to their high structural quality the Fe/Mo(110) islands are particularly suited for this investigation. A comparable quality would be diffult to achieve with lithographically fabricated samples, especially for particles of such elevated thickness. The well-defined shape and structure of the self-assembled islands ensures that the magnetization distribution in the particle is governed by the spatial confinement, and not by roughness effects or by other structural inhomogeneities. However, the consideration of these islands as *model systems* for the magnetization in thick, structured magnetic particles is only valid if the details of the particle shape (e.g., the inclination angle of the facets or the precise hexagonal shape) are not of decisive importance for the resulting magnetic structure. Else, each particle would have its own characteristic magnetic structure depending on its shape, thus precluding an extraction of valuable information of general validity. As will be shown in Sec. VII B, computer simulations demonstrate that the aspect ratio, the size and the thickness are the most important parameters, while details of the shape play only a minor role concerning the overall magnetization structure.

III. EXPERIMENTAL SETUP

The experimental investigation of the magnetic structures was performed with XMCD-PEEM.[35] The principle of XMCD-PEEM is the spin- and helicity-dependent cross section for photoelectron emission with circularly polarized x rays. The lateral resolution of this technique is now better than 30 nm,[36] so that detailed images of the domain structure in mesoscopic elements can be obtained. The experiments have been carried out at the nanospectroscopy beamline of the ELETTRA synchrotron radiation facility.[37] The combination of low-energy electron microscopy (LEEM) and PEEM at ELETTRA makes it possible to image both the morphology and the magnetic structure with the same instrument. In the XMCD-PEEM mode, the samples have been illuminated with monochromatic, elliptically polarized x rays in a microspot of 20×5 μm^2 (in the horizontal and vertical direction, respectively). The local photoelectron current density was imaged with PEEM. The photoelectron density is proportional to the magnetodichroic signal $\boldsymbol{\sigma}\cdot\boldsymbol{M}$, where $\boldsymbol{\sigma}$ is a vector that indicates the direction of the incident light and its helicity and $\boldsymbol{M}$ is the local magnetization vector. Areas with $\boldsymbol{M}$ parallel or antiparallel to $\boldsymbol{\sigma}$ have different secondary electron yields, which leads to a bright and dark contrast. In most cases, we have chosen an irradiation direction $\boldsymbol{\sigma}$ perpendicular to the magnetization direction $\boldsymbol{M}$ in the major domains. Although in this case the major domains show no magnetic contrast, this choice of the beam direction is advantageous because the particularly interesting regions that separate the domains, i.e., the domain walls, display a strong magnetodichroic signal. The imaging of the domain walls requires a very high spatial resolution. In the energy range of the Fe $2p_{3/2}$ (L_3) absorption edge, the photon flux in the illuminated

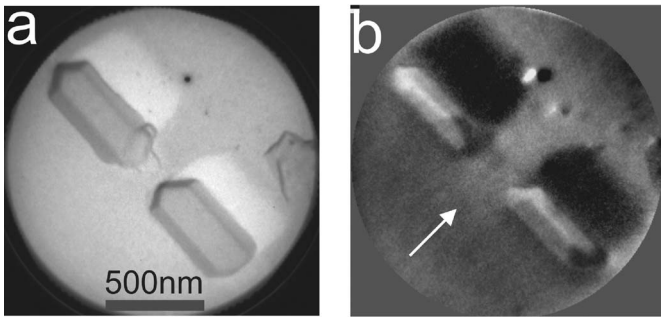

FIG. 2. Example of an experimental observation of the particle shape and the magnetization structure. (a) Two Fe islands, incidentally located next to each other, imaged with LEEM. (b) The XMCD-PEEM image displays the in-plane magnetization component parallel to the incident beam. The beam direction is sketched by the white arrow. Due to grazing incidence of the photons (74° with respect to the plane normal) the back side of the island is shadowed; thus it appears dark in the XMCD-PEEM image.

area is about 10^{11} photons per second, which allows for a fast acquisition of single images, in the range from 10 s to 30 s for images with a field of view of 2.5 μm diameter. The best lateral resolution in XMCD-PEEM mode has been achieved by recording series of about 30 images for each photon beam helicity. The images are postprocessed using a self-correlation algorithm[55] to minimize drift effects. Finally, the magnetic contrast is obtained by subtracting graphically the two accumulated images at opposite light helicities. The magnetic domain configurations have been correlated to the precise morphology of the nanostructures using LEEM. The contrast in LEEM is determined by the surface topography and its crystalline structure. In addition to the diffraction contrast, the so-called interference contrast allows one to image surface steps and thickness gradients in thin films with atomic depth sensitivity and a lateral resolution of few tens nm. This LEEM interference contrast allowed us to unambiguously determine the geometry of the self-organized Fe nanostructures and of their surrounding 45° inclined facets. The quantitative values extracted from the LEEM images (islands' shape, length, width and height) served as input for the micromagnetic simulations. A typical LEEM image and an XMCD-PEEM image of the same sample are shown in Figs. 2(a) and 2(b), respectively.

IV. MICROMAGNETICS AND NUMERICAL METHOD

In the framework of micromagnetism the magnetization inside the sample is represented as a directional field $\boldsymbol{M}=\boldsymbol{M}(\boldsymbol{r})$ with the constraint $|\boldsymbol{M}|=M_s=\text{const}$, where M_s is the saturation magnetization. For a description of the intrinsic properties of the magnetic material, a set of material constants is used. Besides the saturation magnetization M_s, the exchange constant A and the anisotropy constant K are required. The material parameters are connected with micromagnetic energy terms. In our case of magnetic particles with cubic anisotropy in absence of an external magnetic field, the relevant energy terms are the exchange energy

$$E_{\text{exc}}=\int_{(V)} A[(\nabla m_x)^2+(\nabla m_y)^2+(\nabla m_z)^2]dV, \tag{1}$$

the cubic anisotropy energy

$$E_{\text{cub}}=\int_{(V)} K_c(\alpha_1^2\alpha_2^2+\alpha_1^2\alpha_3^2+\alpha_2^2\alpha_3^2)dV \tag{2}$$

and the stray field energy

$$E_{\text{stray}}=-\frac{\mu_0}{2}\int_{(V)} \boldsymbol{M}\cdot\boldsymbol{H}_s dV. \tag{3}$$

We have used $K_c=4.8\times10^4$ J/m^3, $A=2.0\times10^{-11}$ J/m, and $M_s=1.73\times10^6$ A/m to describe the material of the Fe islands. The easy axes are oriented along the [001], [100], and [010] directions; cf. Fig. 1(b). In Eq. (1) $\boldsymbol{m}=\boldsymbol{M}/M_s$ is the normalized (reduced) magnetization, and in Eq. (2), α_1, α_2, and α_3 are the directional cosines of the magnetization $\boldsymbol{M}$ with respect to the cubic easy anisotropy axes. These material parameters lead to a quality factor $Q=2K/\mu_0M_s^2\simeq2.5\times10^{-2}$. A value of $Q\ll1$ indicates that the material is magnetically soft, i.e., that the arrangement of the magnetization is primarily driven by the need to minimize the demagnetizing energy rather than the anisotropy energy.[56] In Eq. (3), $\boldsymbol{H}_s=-\nabla U$ is the stray field and U is the magnetic scalar potential. The potential U satisfies Poisson's equation $\Delta U=\rho/\mu_0$ inside the sample volume V and the Laplace equation $\Delta U=0$ outside the sample. The volume charges $\rho=\mu_0\nabla\boldsymbol{M}$ and the surface charges $\sigma=\boldsymbol{n}\cdot\boldsymbol{M}$ ($\boldsymbol{n}$: outward surface normal vector) are the sources of the stray field. The reduction or avoidance of these charges lowers the stray field energy.[7] For the inward limit U_i and the outward limit U_o of the potential at the surface, the Neumann boundary conditions at the surface ∂V read

$$\left.\frac{\partial U_i}{\partial \boldsymbol{n}}\right|_{\partial V}-\left.\frac{\partial U_o}{\partial \boldsymbol{n}}\right|_{\partial V}=\sigma. \tag{4}$$

In addition, the boundary condition $\lim_{x\to\infty}U(x)=0$ has to be fulfilled. Details on the numerical calculation of U by means of a combined boundary element–finite element method are given elsewhere.[38]

If the material parameters and the anisotropy axes are specified, the magnetic energy of the sample is uniquely determined by the magnetization distribution $\boldsymbol{M}(\boldsymbol{r})$. In the static equilibrium, the magnetization arranges in a way to minimize the total energy $E_{\text{tot}}=E_{\text{exc}}+E_{\text{cub}}+E_{\text{stray}}$. In the computer simulation, the minimization is performed by using the conjugate gradient method.[39] The minimization has to be performed under the constraint $|\boldsymbol{M}|=M_s$, which can be easily ensured by representing the local magnetization direction with spherical coordinates ϑ and φ.

The numerical representation and the micromagnetic modelling is performed with the finite element method (FEM), using a code developed by Hertel.[38] In the finite element representation, the sample's volume is subdivided into tetrahedral elements of irregular size and shape. The magnetization is discretized at the corner points of the elements (the nodes). A piecewise linear representation of the

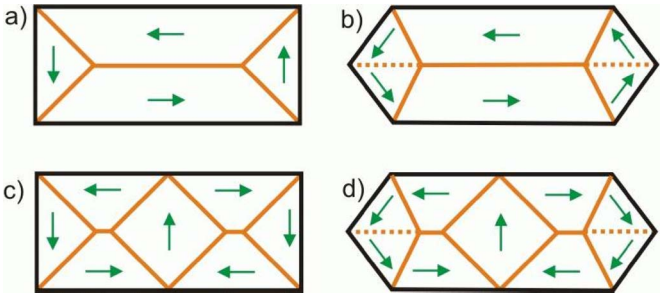

FIG. 3. (Color online) Simple magnetic-flux-closure patterns in thin-film elements. (a), (c) Landau and diamond structure in a rectangle, respectively; (b), (d) modified Landau and diamond structure, respectively, in a hexagonal particle. In the hexagonal element, the closure domains are subdivided in two regions separated by an additional domain wall (dashed line).

magnetization is obtained by means of normalized, linear interpolation functions that are defined in each element (the so-called shape functions). The FEM is a particularly powerful and accurate technique for micromagnetic simulations. It allows the smooth modelling of particles of general geometry (with curved or inclined surfaces) and gives the possibility to apply adaptive mesh refinement techniques. These unique features of the FEM are of essential importance for the present study where large samples with a complicated shape are modeled.

V. THE VAN DEN BERG SCHEME

In thin-film elements, magnetic flux-closure patterns are relatively simple and well known. The Landau pattern and the diamond pattern (cf. Fig. 3) are typical examples thereof. Such flux-closure patterns are determined by the particle's boundary and the tendency to avoid magnetic surface charges. In sufficiently large soft-magnetic thin-film elements, the magnetization is oriented in the film plane and is locally aligned parallel to the particle edges. This avoidance of magnetic surface charges gives rise to the formation of magnetic domains. The Van den Berg scheme[5,40,41] is a simple graphical method for the construction of flux-closure patterns in thin-film elements of arbitrary shape. This method is derived from a rather complicated mathematical analysis that assumes an idealized model for two-dimensional thin film elements with (a) no magnetic anisotropy, (b) perfect avoidance of magnetic charges, and (c) domain walls of vanishing width. According to this scheme, the center point of each circle that touches the particle's boundary at least twice is placed on a domain wall. This construction scheme generally leads to symmetric domain structures, that, despite the idealizations assumed in the model, correspond very well to domain structures as they are obtained in experiments[4] and micromagnetic simulations.[11,42] The Van den Berg scheme was also found to be valid in self-assembled Fe/Mo(110) elements of moderate thickness ($t \lesssim 60$ nm).[22] In our thicker samples, however, we observe flux-closure domain structures that differ significantly from the Van den Berg scheme. It should be noted that the occurrence of deviations from the Van den Berg in thick particles is, *per se*, not surprising, since the scheme has been derived using a thin-film approximation. A comparable scheme has not yet been reported for three-dimensional samples. Analytic studies on the magnetic structure in three-dimensional magnetic structures have been reported by Arrott *et al.*,[43,44] which were, however, restricted to special particle shapes. In this paper we report on systematic, qualitative deviations from the Van den Berg scheme in particles of elevated thickness. In order to highlight these differences, we shall refer to the idealized flux-closure pattern according to Fig. 3(a) as the *classical* Landau structure, which will serve us as a paradigm for magnetic domain structures in thin-film elements. This term is coined with reference to the original work by Landau,[45] where the internal wall structure had been neglected. The classical Landau structure is a flux-closure domain pattern in rectangular samples. It contains four 90° walls and one 180° domain wall in the middle. The domain walls are assumed to be straight, thin lines. The 90° walls extend from the corners to the central 180° wall, which is parallel to the long edge of the rectangle and with which they enclose an angle of 135°. To a very good approximation, this pattern corresponds to experimental observations of domain structures in rectangular magnetic platelets. But also in particles of non-rectangular shape and even in extended films[46] this type of structure has been observed. In a hexagonal particle, the four-domain Landau in a rectangle turns into a structure with six domains [cf. Fig. 3(b)]. A distinction between this structure with six domains and the Landau pattern may be neglected since the domain pattern is very similar to the classical structure with four domains: two major domains and two closure domains. Therefore, such modified variants also have been reasonably labeled as "Landau structure," or sometimes as "Landau-type structure" in the literature, in spite of more or less pronounced differences from the classical structure. In our case of thick particles, however, the differences are significant and we require a different wording. Our study suggests that in the three-dimensional case, the classical Landau structure is replaced by a complex flux closure pattern with characteristic features. We shall call this the *generalized* Landau structure and we will discuss this structure in detail in Sec. VII A.

VI. RESULTS

A. Asymmetric flux-closure patterns

We have taken LEEM and XMCD-PEEM images of the magnetization at zero field of about thirty Fe islands. In all cases, flux-closure magnetization patterns have been observed.

Figure 4(b) shows an example of a typical domain pattern observed in the experiments. The grey scale displays the y component of the magnetization, i.e., the projection of the magnetization at the surface along the polarization of the incident beam. The magnetic structure in Fig. 4(b) is clearly subdivided into domains, but the shape of the domains is not in accordance with the Van den Berg scheme, as can be seen by comparing Fig. 4(c) and Fig. 4(d). The grey scale in these schematic drawings refers again to the y component, so that the dashed domain walls sketched in Fig. 4(c) would not be visible in this experiment, since they separate regions of dif-

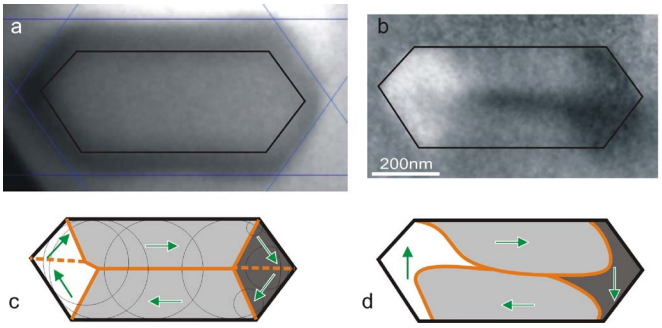

FIG. 4. (Color online) Difference between idealized and observed magnetic domain structure. (a) LEEM image of the sample shape. XMCD-PEEM image of the magnetic domain structure. (c) Schematic domain structure for the given shape according to the Van den Berg scheme. (d) Approximate shape of the magnetic domains according to the experimental observation.

ferent magnetization direction with the same value of m_y. Similar to the classical Landau structure, the magnetization distribution in Fig. 4(b) is split into four domains: two major domains where the magnetization is parallel to the long edge and two closure domains that connect the magnetic flux between the major domains. However, neither the shape of the domains nor the position of the domain walls corresponds to the Van den Berg scheme.

We have found such distorted, asymmetric domain patterns bearing only a weak resemblance to the classical Landau structure in all the particles that we have investigated, as we will discuss in Sec. VI C. The reason for the asymmetric structures and the deviations from the Van den Berg scheme lies in the three-dimensional nature of these particles.

B. Micromagnetic simulations

The XMCD-PEEM experiments only provide information about one magnetization component (the component parallel to the incident beam) on the flat, topmost surface of the sample. Therefore, numerical simulation methods are employed to investigate the internal structure of the magnetization. The simulation results are cross-checked with the experimental observations to guarantee that the simulated structures correspond to the observed ones.

Simulating the magnetization in these particles is problematic because of their size, which is enormous from the point of view of computational micromagnetism. In particles of large size, it is difficult to avoid discretization errors that result from too large discretization cells. The consequence of discretization errors is not only a rough representation of the magnetization, but also wrong results due to numerical "domain wall collapse,"[47] i.e., an unrealistic, large change of the magnetization direction within a single disretization cell. To avoid discretization errors, the size of the discretization cells should not exceed the exchange length $\Lambda = \sqrt{2A/(\mu_0 M_s^2)} \simeq 3$ nm. Since the particle volume is of the order of 1 μm^3, simulations with a regular grid would require an unsustainably large number of several millions of discretization cells. An adaptive mesh refinement technique[48] has been employed to solve this problem. Such adaptive

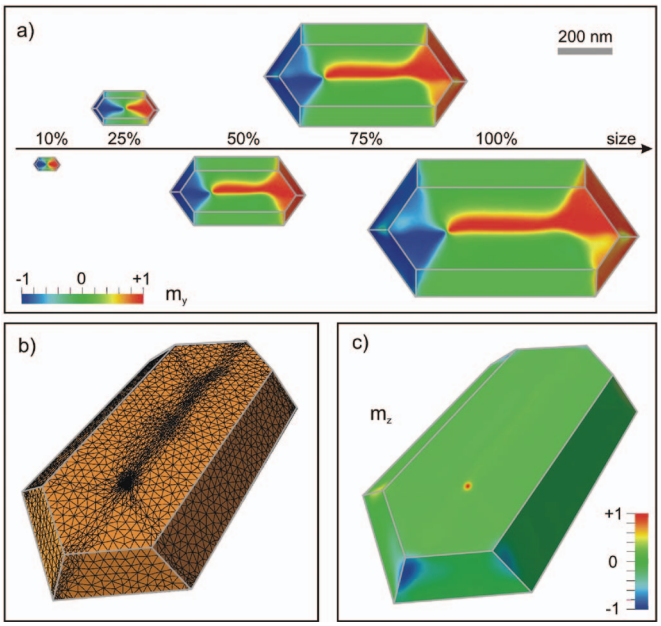

FIG. 5. (Color) To avoid discretization errors in the simulation of the three-dimensional magnetic domain structure, the sample is first reduced to a tenth of its size. By using cycles of micromagnetic energy minimization and three-dimensional adaptive mesh refinement, the sample is gradually increased to its real size (a). After this procedure, a finite-element mesh with regions of strongly different discretization density is obtained (b). The finite elements are particularly small in regions of strong magnetic inhomogeneities (vortices, domain walls). Owing to the mesh refinement, even the nanometric vortex core with magnetization perpendicular to the surface is fully resolved, as can be seen in the red spot in panel (c). Throughout the paper, unless otherwise specified, the color coding used to represent a component of the reduced magnetization $\boldsymbol{m}$ is chosen according to the bar on the bottom of panel (a).

methods are particularly powerful for static micromagnetic simulations of large particles, where the inhomogeneities of the magnetization are limited to a small fraction of the sample's volume. These regions, i.e., the domain walls, require a high discretization density, whereas large domains with homogeneous magnetization can be calculated safely with a coarse mesh. Therefore, adaptive refinement methods allow for accurate numerical results while keeping the computational costs (processing time, memory) low.

The procedure we have applied for the micromagnetic simulations is as follows. First, the exact geometrical shape of each Fe island is extracted from LEEM images and a corresponding finite element model is constructed. Subsequently, the model is scaled down to 1/10 of its actual size. The magnetization distribution in this small island is simulated by means of energy minimization, using a symmetric vortex structure around the center as initial configuration. Once a converged solution is found, the mesh is adaptively refined and the equilibrium structure is calculated with the refined mesh. The cycle of mesh refinement and energy minimization is repeated until the maximum angle enclosed between the magnetization vectors at two neighboring discretization points drops below $\pi/10$. Then, the size of the sample is increased, and the procedure of mesh refinement and en-

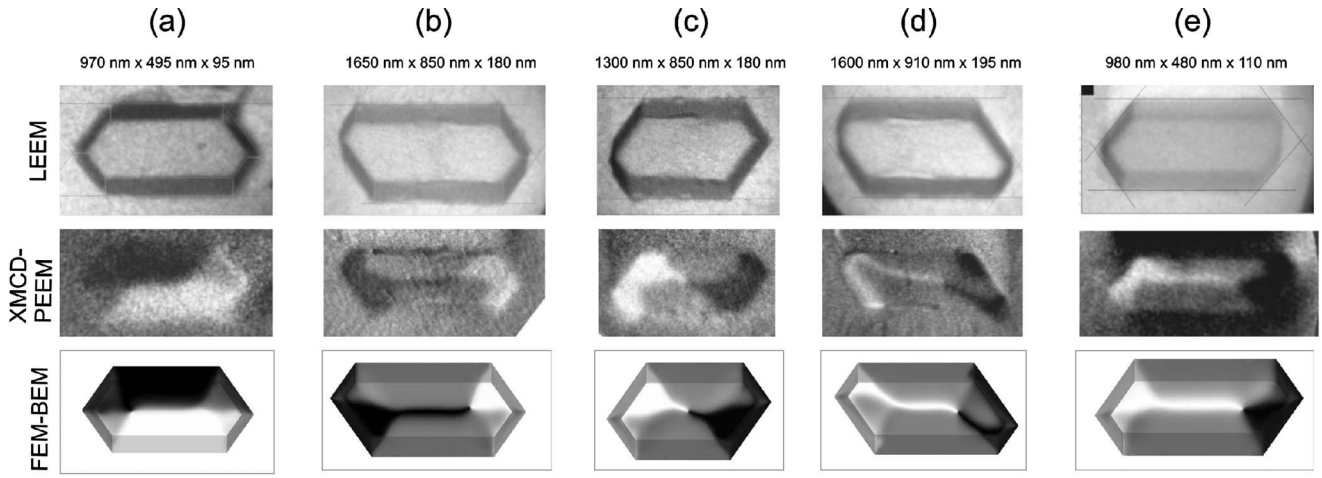

FIG. 6. Experimental and simulated data for five self-assembled Fe/Mo(110) islands of different size and shape (a)–(e). *First row*: The shape of the particle is obtained by LEEM imaging. The particle thickness is derived from the width of the (001) facets, which appear as a dark border around the hexagonal top surface, by using the known inclination angles of the inclined facets (cf. Fig. 1). The sample's approximate lateral dimension and thickness is displayed on top of each column. *Second row*: One magnetization component in the surface plane is imaged as grey scale with XMCD-PEEM. In sample (a), the contrast refers to the magnetization component parallel to the long edge while in the other samples the in-plane magnetization component perpendicular to the long edge is displayed. Notice that only the top surface, i.e., the light grey internal hexagon in the first row, is imaged. *Third row*: Micromagnetic simulation results. To compare the results with the XMCD-PEEM experiments, the same magnetization component is displayed in grey scale. The sample shape was modeled according to the LEEM images and the model explained in Fig. 1.

ergy minimization is repeated. With this iterative process, the sample size is increased in small steps towards its real value and the mesh is progressively refined. This way of slowly "inflating" the sample guarantees that the magnetic structure is calculated without discretization errors. The simpler variant of simulating the magnetic structure directly with a coarse mesh, without reducing the sample's size, and subsequently applying the mesh refinement procedure is less accurate because the first calculation would lead to large discretization errors. Especially in three-dimensional calculations, it is advisable to prevent discretization errors rather than trying to remove them *a posteriori*. An example for the simulation of the magnetization by means of stepwise increase of the sample size is shown in Fig. 5(a). The typical cell size of a refined mesh is between about 25 nm in the homogeneous regions and 1.5 nm in the refined regions. By increasing the sample size, we find that the symmetric vortex structure in small particles evolves to an asymmetric domain structure above a certain sample size. Such a transition can be seen in Fig. 5(a), where the asymmetry occurs after the sample has been increased to 50% of its actual size. The formation of the asymmetric structure obviously involves a breaking of symmetry: the vortex which is originally placed in the center may either shift to the right or to the left side on the top surface. As will be discussed later, the sign of the perpendicular component in the vortex core may also have a strong influence on the resulting domain structure.

C. Comparison between experiment and simulation

The simulation results are in excellent agreement with the experimental data. A number of examples are shown in Fig. 6. The experimentally observed asymmetric shape of the end domains and the position of the domain walls are reproduced almost perfectly by the simulations. All the unexpected features of the domain patterns and their deviation from the Van den Berg scheme occur in just the same way in both the experiment and the simulations. Notice that all these details of the magnetic structure develop automatically in the simulation by using a simple vortex as a starting configuration.

The one-to-one correspondence between experimental and simulated surface magnetization is a strong indication that the simulated structures are indeed equal to the experimental ones. Therefore, the simulations can be used to obtain information that is not directly accessible in the experiment, i.e., the three-dimensional structure of the magnetization inside the sample. The investigation of the inner structure of the magnetization is a prerequisite for the explanation of the unexpected experimental results.

VII. DISCUSSION

A. Internal domain wall strucure

The magnetization distribution inside the sample differs significantly from the distribution observed at the surface. A typical example is shown in Figs. 7(a)–7(c) that displays the y component of the magnetization on three cross sections at the top ($z=t$), the middle ($z=t/2$) and the bottom ($z=0$), respectively. The coordinate frame is chosen according to Fig. 1. In the middle cross section, the domain pattern is almost symmetric and in good agreement with the Van den Berg scheme, while on the top and the bottom the structure is clearly asymmetric. The twist is in opposite directions on the top and the bottom surface; cf. Figs. 7(a) and 7(c). The inhomogeneity of the magnetization along the z direction and

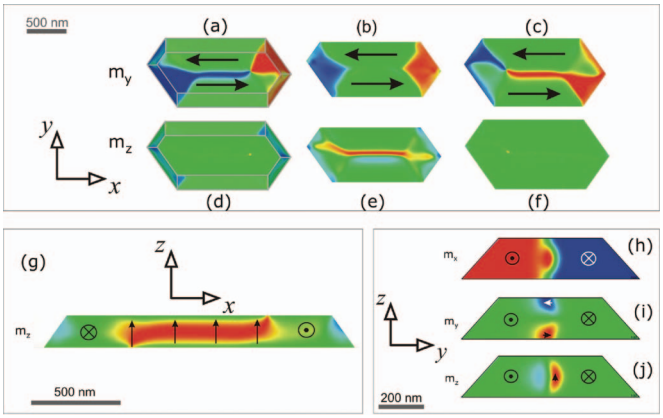

FIG. 7. (Color) Magnetization distribution on different cross sections. The example shown here refers to the particle displayed in Fig. 6(b). Figures (a) and (d) show the top view on the three-dimensional sample with lateral facets. (b),(e) Cross section through the middle of the sample at $z=t/2$; (c),(f) magnetization on the bottom surface of the sample, $z=0$. (g) m_z component on the cross section through the middle of the sample parallel to the xz plane. (h)–(j) Asymmetric Bloch wall: magnetization components on a cross section at midlength, parallel to the yz plane.

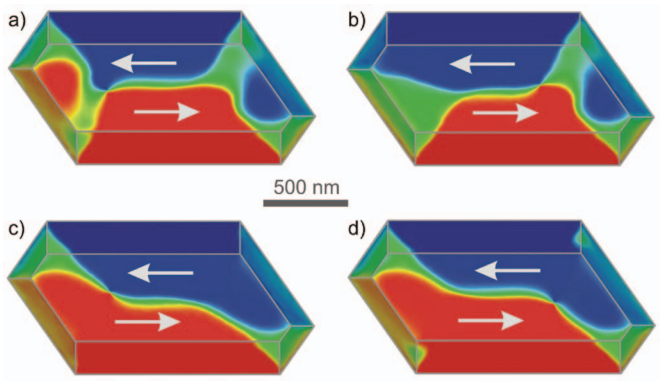

FIG. 8. (Color) Simulation of four different configurations in a sample of identical shape. The shape and the size of the sample is the same as in Fig. 6(d). Although topologically the structure is very similar in all cases (Landau structure with asymmetric Bloch wall), the resulting magnetic patterns are significantly different. In the structures (a) and (b) the Bloch component of the internal wall, m_z, is positive, whereas in (c) and (d) it is negative. The structures (a) and (c) have the same direction of the magnetization in the Néel caps, m_y, which is opposite to the orientation in the structures (b) and (d).

the resulting asymmetry in the top and bottom xy plane result from the formation of an asymmetric 180° Bloch wall:[26,49] in the middle of the sample ($z=t/2$) the major domains are separated by a Bloch wall, while on the top and bottom surface, the transition between the major domains is given by a Néel wall (the so-called Néel caps). In a cross section on a plane with $x=$const through the middle of the sample, the typical profile of an asymmetric Bloch wall resulting from the combination of Bloch and Néel wall can be clearly seen in Figs. 7(h)–7(j). There are different possibilities for the orientation of the magnetization in this type of domain wall: The magnetization in the Bloch part can point either in the positive or in the negative z direction, and the magnetization in the Néel caps can point either in the positive or negative y direction. The orientation or the chirality of the asymmetric Bloch wall can have a strong impact on the resulting domain structure, as shown in Fig. 8. Depending on the direction of the magnetization of the Néel caps and the direction of the inner Bloch component, the magnetic domain structure on the surface may be very different. In the example shown in Fig. 8, the computer simulation first yielded the structure (a) for this geometry. In the simulations, the aforementioned breaking of symmetry that is involved with the formation of such structures results from numerical roundoff errors and the direction in which the Néel caps evolve is impredictable. This imponderability can be removed by breaking the symmetry with an oblique, weak external field that is applied during the simulated expansion of the sample; cf. Fig. 5(a). With this controlled breaking of symmetry we obtained the structures shown in Fig. 8, including the structure (d), which almost perfectly reproduces the experimental observation, cf. Fig. 6(d). Apart from possible minor differences concerning the out-of-plane component of the magnetization along the facets, there are four main types of such almost degenerate structures, corresponding to the two possibilities for the orientation of the Bloch component and the Néel caps, respectively.[57] In a sense, these structures can be compared to geometric isomers of a molecule: The domain structures contain the same components (Landau structure with asymmetric internal walls), but the orientation is different (opposite orientation of the Néel caps and/or of the Bloch wall). The domain structures of such "isomers" can differ significantly in their patterns on the surface, especially if the sample shape is strongly asymmetric.

In any case, the Néel caps of an asymetric Bloch wall are oriented in opposite direction on opposite surfaces. The formation of an asymmetric Bloch wall represents an energetically optimized arrangement concerning the stray field energy. Magnetostatic volume charges $\rho=\mu_0\nabla\boldsymbol{M}$ are largely avoided by the formation of a Bloch wall in the center of the sample and surface charges $\sigma=\boldsymbol{M}\cdot\hat{\boldsymbol{n}}$ ($\hat{\boldsymbol{n}}$: surface normal vector) are effectively suppressed by the Néel caps. Depending on whether the magnetization in the Néel caps is pointing parallel or antiparallel to the magnetization direction in the closure domains (the domains close to the particle's border in the $\pm x$ direction), the Néel caps are either connected smoothly to the closure domain or separated by them with a

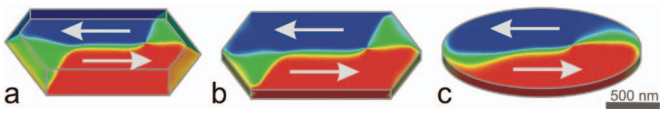

FIG. 9. (Color) Geometry dependence of the magnetization structure in a three-dimensional island. (a) Perspective view on the simulated magnetization structure of the particle shown in Fig. 6(b). (b) Simulated magnetic domain structure in a particle of same size and thichkness, but with symmetric in-plane shape and vertical facets. (c) Even if the hexagonal shape is replaced by a smooth elliptical boundary, the magnetization structure remains almost unchanged, with the same asymmetric characteristics.

magnetic vortex, respectively.[50] Inside the closure domain, on cross sections with constant value of x, the structure is similar to an asymmetric Néel wall. The main difference between an asymmetric Néel wall and an asymmetric Bloch wall is the relative orientation of the magnetization in the Néel caps, being parallel in the former and antiparallel in the latter. It has been predicted, by means of numerical simulations, that the combination of asymmetric wall types in mesoscopic, soft-magnetic particles leads to a pronounced in-plane asymmetry on the top surfaces.[18,51] Our XMCD-PEEM investigations on several mesoscopic Fe islands clearly confirm this prediction and provide a direct observation of this effect.

B. Shape dependence

In the numerous particles that we have investigated, we have almost exclusively found the Landau-type flux-closure pattern described above, the *generalized* Landau structure. A few exceptions of different magnetization arrangements will be discussed in the next sections. The generalized Landau structure consists of four domains, two major domains that are connected by an asymmetric Bloch wall and two closure domains connected to the major domains by 90° walls. Our observation of the Landau structure in self-assembled Fe islands with their quite complicated hexagonal shape and the inclined facets suggests that the formation of this arrangement of the magnetization is rather driven by the particle's aspect ratio and its size than by the rectangular shape.

The question arises to which extent the asymmetric Landau pattern that we observed is specific to our example of hexagonal particles with inclined facets. How sensitively does the magnetic structure depend on the precise shape of the particle? To answer this question, the influence of the particle shape on the resulting magnetic domain structure has been investigated with micromagnetic simulations. Unlike the real world, where the shape of the Fe islands is determined by the energetics of the growth mode, finite element models give the possibility to study magnetic structures in mesoscopic particles of arbitrary shape. Starting from a "real" island, i.e., one that is modelled exactly according to the experiment, we have first tested to which extent the magnetic pattern is affected by the inclined facets and the asymmetry of the hexagon. This has been done by simulating the magnetization in a hexagonal particle of same thickness and size, but with symmetric hexagonal shape and a "cookie-cutter" geometry, i.e., an island with perpendicular facets. The result is displayed in Fig. 9(b). The asymmetric magnetic structure is practically the same as it has been observed in the real island with inclined facets, indicating that neither the inclination of the facets nor the asymmetry of the hexagon has a decisive impact on the magnetic structure. To further check whether the hexagonal shape is of importance for the resulting magnetic structure, a flat, elliptical particle has been modelled. The major axes of the ellipse (parallel to the x and y direction, respectively) correspond to the width and length of the original island and the thickness is again the same. The result [Fig. 9(c)] shows that the distorted Landau structure also occurs in this particle. Recent studies[58] show that practically the same structure may also be found in an ellipsoidal particle of comparable size and aspect ratio. These computer experiments indicates that the generalized Landau structure is hardly determined by the particle shape. This is in contrast to two-dimensional samples, where the essential importance of the sample shape reflects in the Van den Berg construction scheme, where the domain structure is determined *exclusively* by means of the particle shape. The occurrence of the three-dimensional, generalized Landau structure is neither restricted to particles of rectangular, hexagonal or any other specific shape; not even to flat particles. In the three-dimensional case, it is rather the thickness, the size and the aspect ratio that are decisive. The primary tendency of the magnetization in thick, three-dimensional particles appears to be to develop an asymmetric 180° Bloch wall, while in the case of thin-film elements, the major domains may either be separated by a 180° wall (classical Landau structure) or by 90° walls (diamond state).

C. Diamond structure

By far, the magnetization states that we have observed most frequently are the above-mentioned variants of the Landau structure. The absence of the "diamond state" in these thick elements is remarkable. The diamond state is an alternative flux-closure pattern with seven domains (cf. Fig. 3) that is frequently observed in thinner soft-magnetic particles[22,33,51] of similar size.

We suspect that the predominance of the Landau structure and the absence of the diamond state can be explained with energetic considerations in connection with the elevated particle thickness. The thickness dependence of domain configurations in nanoscale Fe/W(110) islands of significantly lower thickness (ca. 3–8 nm) has been studied recently by Bode *et al.*[52] In the present case, the idea is the following. Essentially, the Landau structure has one central 180° wall and four 90° domain walls, whereas the diamond structure consists of seven domains that are separated by *eight* 90° domain walls. While in the case of a 180° wall magnetic volume charges can efficiently be avoided by the formation of an asymmetric Bloch wall, a 90° wall inevitably contains volume charges $\rho = \nabla \boldsymbol{M}$, like a Néel wall does. With increasing thickness, the energy connected with these volume charges increases and so does the tendency to avoid them. The tendency to avoid these charged 90° walls and, instead, to form a 180° wall, favors the formation of the Landau structure over the diamond structure. If this consideration is correct, the tendency to avoid the diamond state should decrease with decreasing thickness. We therefore searched for the diamond state in islands of large in-plane extension (to ensure that the particle is in a multidomain state) that were particularly thin. In our set of samples the typical thickness was about 100–150 nm, but we eventually found an island of 65 nm thickness and about 1000 nm $\times$ 500 nm lateral extension. The XMCD-PEEM investigation of the magnetization in this island indeed showed that the sample was magnetized in the diamond state; cf. Fig. 10. This sample is the only one in which we found the diamond state. The fact that we have observed this state only after a selective search

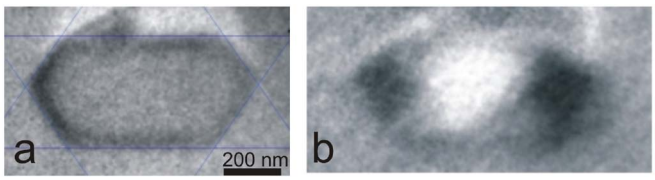

FIG. 10. (Color online) In a relatively large and particularly thin island, identifiable as such in a LEEM image (a) by the thin dark boundary (the lateral facets), a "diamond state" magnetization structure was found. The diamond state is characterized by two vortices with opposite vorticity and a diamond-shaped central domain, which is clearly recognizable on the right panel (b).

aimed at finding particularly thin elements suggests that the thickness, actually, plays a decisive role. Further studies are required to systematically analyze this suggested thickness dependence of magnetization states.

D. Vortex structure

Besides the thickness and the size, also the in-plane aspect ratio has an impact on the resulting magnetization state. This can be seen by comparing the magnetic structure of two islands of similar thickness and width, but different length, cf. Figs. 6(b) and 6(c). In one case, the aspect ratio (length in x direction vs width in y direction) is 2.1 and in the other it is about 1.5. The particle with lower aspect ratio has a vortex in the center of the sample. It contains no asymmetric Bloch wall and the closure domains are asymmetric and twisted. They are stretched in the x direction and they join in the middle of the sample at the vortex. In contrast to this, the longer sample has a clearly developed 180° domain wall in the middle which separates the major domains. Obviously, a sufficiently large particle with aspect ratio approximately equal to one would not form a Landau structure with a central 180° domain wall, but would be magnetized in a simple vortex state with a magnetic vortex structure in the centre of the sample. With increasing aspect ratio, the vortex core is stretched until it eventually performs a kink through the sample and forms the center of an asymmetric Bloch wall. Thus, by changing the aspect ratio, a transition from a vortex state to a generalized Landau structure occurs at a critical size. Whether this transition is continuous or discontinuous may be the subject of future studies.

E. Bloch switch

In most cases the simulations yield magnetic structures that agree very well with the ones that have been observed in the experiments, but occasionally some interesting differences between simulation and experiments have occurred. The possible differences concerning the chirality of the asymmetric central Bloch wall have already been discussed in Sec. VII A. Another variant of the Landau structure was obtained in one case, where the simulation has yielded a structure as shown in Figs. 11(b) and 11(c). Instead of the usual straight line, the central domain wall (i.e., the Néel cap) displays a pronounced kink. It is known from studies of asymmetric domain walls in extended magnetic films that

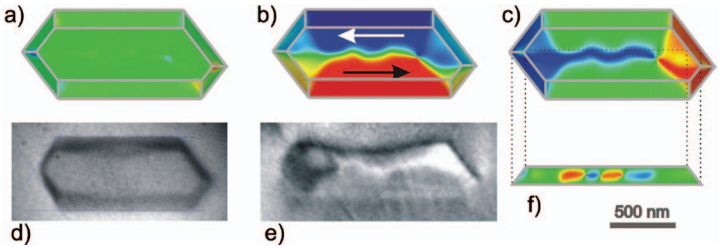

FIG. 11. (Color) (a)–(c) z, x, and y component of the magnetization of a simulated magnetic domain structure with undulated central domain wall. (f) z component of the magnetization on a cross section of constant y. The alternating red-blue regions indicate switches of the Bloch component. (d) LEEM image and XMCD-PEEM image (e) of a sample in an apparently similar magnetization state. The size of the island is 1500 nm × 620 nm × 130 nm.

such a kink is characteristic for a so-called Bloch switch.[5,53] A Bloch switch is given when the sign of the Bloch component changes along the domain wall inside the film, while the magnetization direction of the Néel caps remains unchanged. In fact, a look at the inner part of the simulated magnetization structure [Fig. 11(f)] shows that the arrangement contains Bloch switches. We have also observed a similar kink in the experiment, as shown in Fig. 11(e).

This example is the only island in which we have found this kink experimentally, and it can therefore not be ruled out that the kink may have other reasons than a Bloch switch like, e.g., a structural inhomogeneity of the island. Moreover, the top surface of the island in which we observed the kink was not ideally flat, as could be seen by the shadow of the island as described in Fig. 2(b). Due to these deviations of the sample morphology from the ideal construction scheme according to Fig. 1, the model for the island shape that has been used in the simulations that yielded a Bloch switch does not correspond exactly to the island in which the kink has been observed experimentally. Therefore, although a correspondence between experiment and simulation is likely, the available data from simulation and experiment are not sufficient for an unambiguous proof that the kink results from a Bloch switch. The results, however, suggest that an asymmetric Bloch wall with a Bloch switch may develop also in patterned particles and that such a Bloch switch would lead to a considerable distortion of the otherwise straight central domain wall. To our knowledge, this kind of domain wall has not been reported previously in patterned elements.

VIII. CONCLUSIONS

"The simplest problem in continuum magnetism in a singly connected finite body is the Landau structure (…), but it remains an unsolved problem to describe it in all its details." This is a quote from a paper by Arrott and Templeton[50] that was written in 1997, at a time when the experimental resolution was not yet sufficient for a direct observation of details of the magnetization and most micromagnetic simulation methods were not accurate enough for large, three-dimensional computations.[59] Owing to the combination of (a) advanced growth methods yielding high-quality, monoc-

rystalline mesoscopic Fe particles that can be regarded as model systems, (b) LEEM imaging to obtain detailed information on the particle shape, (c) high-resolution XMCD-PEEM studies that provide information on the in-plane manetization at the particle surface, and (d) accurate FEM/BEM micromagnetic modeling with adaptive mesh refinement techniques providing a detailed model of the three-dimensional magnetization structure, we have obtained a full description of the Landau structure. The Landau structure seems to occur as a minimum energy arrangement in soft-magnetic particles of very different shape. Generally, the size, thickness, and aspect ratio are more important for the formation of the generalized Landau structure than details of the particle's shape and its surfaces. The fascinating complexity of the Landau structure occurs when the particle is thick enough to sustain an asymmetric Bloch wall. The classical, symmetric Landau pattern occurring in rectangular thin film elements can be regarded as a simple thin-film limit of a more general, three-dimensional structure. In the thin-film limit, the central asymmetric Bloch wall is replaced by an ordinary Néel walls, thus simplifying drastically the arrangement.

ACKNOWLEDGMENTS

We acknowledge financial support from the EU VI Framework Program Transnational Access [RII3-CT-2004-506008(IA-SFS)] and Laboratoire Européen Associé (LEA) Mesomag (MPI-Halle/LLN). We thank V. Santonacci and Ph. David for technical support on the UHV growth chambers. We also acknowledge support by the European Community–Research Infrastructure Action under the FP6 "Structuring the European Research Area" Programme (through the Integrated Infrastructure Initiative "Integrating Activity on Synchrotron and Free Electron Laser Science").

*Electronic address: r.hertel@fz-juelich.de

[1] J. I. Martín, J. Nogués, K. Liu, J. L. Vicent, and I. K. Schuller, J. Magn. Magn. Mater. **256**, 449 (2003).
[2] R. P. Cowburn, D. K. Koltsov, A. O. Adeyeye, M. E. Welland, and D. M. Tricker, Phys. Rev. Lett. **83**, 1042 (1999).
[3] K. J. Kirk, J. N. Chapman, and C. D. W. Wilkinson, Appl. Phys. Lett. **71**, 539 (1997).
[4] R. D. Gomez, T. Luu, A. Pak, I. Mayergoyz, K. Kirk, and J. Chapman, J. Appl. Phys. **85**, 4598 (1999).
[5] A. Hubert and R. Schäfer, *Magnetic Domains—The Analysis of Magnetic Microstructures* (Springer, Berlin, New York, Heidelberg, 1998).
[6] W. F. Brown, Jr., *Micromagnetics* (Interscience Publishers, John Wiley & Sons, New York, London, 1963).
[7] A. Aharoni, *Introduction to the Theory of Ferromagnetism*, 2nd ed. (Oxford Science Publications, Oxford Clarendon Press, Oxford, 2000).
[8] E. C. Stoner and E. P. Wohlfarth, Philos. Trans. R. Soc. London, Ser. A **240**, 599 (1948).
[9] W. Wernsdorfer, E. B. Orozco, K. Hasselbach, A. Benoit, B. Barbara, N. Demoncy, A. Loiseau, H. Pascard, and D. Mailly, Phys. Rev. Lett. **78**, 1791 (1997).
[10] A. Yamasaki, W. Wulfhekel, R. Hertel, S. Suga, and J. Kirschner, Phys. Rev. Lett. **91**, 127201 (2003).
[11] R. Hertel, Z. Metallkd. **93**, 957 (2002).
[12] N. A. Usov, C. R. Chang, and Z. H. Wei, J. Appl. Phys. **89**, 7591 (2001).
[13] H. Kronmüller, Z. Phys. **168**, 478 (1962).
[14] J. Rothman, M. Kläui, L. Lopez-Diaz, C. A. F. Vaz, A. Bleloch, J. A. C. Bland, Z. Cui, and R. Speaks, Phys. Rev. Lett. **86**, 1098 (2001).
[15] K. Nielsch, R. B. Wehrspohn, J. Barthel, J. Kirschner, U. Gösele, S. F. Fischer, and H. Kronmüller, Appl. Phys. Lett. **79**, 1360 (2001).
[16] M. H. Park, Y. K. Hong, S. H. Gee, D. W. Erickson, and B. C. Choi, Appl. Phys. Lett. **83**, 329 (2003).
[17] K. J. Kirk, S. McVitie, J. N. Chapman, and C. D. W. Wilkinson, J. Appl. Phys. **89**, 7174 (2001).
[18] R. Hertel and H. Kronmüller, Phys. Rev. B **60**, 7366 (1999).
[19] W. Rave, K. Fabian, and A. Hubert, J. Magn. Magn. Mater. **190**, 332 (1998).
[20] J. K. Ha, R. Hertel, and J. Kirschner, Phys. Rev. B **67**, 224432 (2003).
[21] M. Hehn, K. Ounadjela, J.-P. Bucher, F. Rousseaux, D. Decanini, B. Bartenlian, and C. Chappert, Science **272**, 1782 (1996).
[22] P. O. Jubert, J.-C. Toussaint, O. Fruchart, C. Meyer, and Y. Samson, Europhys. Lett. **63**, 132 (2003).
[23] F. Bloch, Z. Phys. **74**, 295 (1932).
[24] L. Néel, C. R. Hebd. Seances Acad. Sci. **241**, 533 (1955).
[25] R. M. Moon, J. Appl. Phys. **30**, 82S (1959).
[26] A. Hubert, Phys. Status Solidi **32**, 519 (1969).
[27] P. O. Jubert, R. Allenspach, and A. Bischof, Phys. Rev. B **69**, 220410(R) (2004).
[28] P. Bruno, Phys. Rev. Lett. **83**, 2425 (1999).
[29] R. D. McMichael and M. J. Donahue, IEEE Trans. Magn. **33**, 4167 (1997).
[30] M. Kläui, C. A. F. Vaz, J. A. C. Bland, L. J. Heyderman, F. Nolting, A. Pavlovska, E. Bauer, S. Cherifi, S. Heun, and A. Locatelli, Appl. Phys. Lett. **85**, 5637 (2004).
[31] O. Fruchart, S. Jaren, and J. Rothman, Appl. Surf. Sci. **135**, 218 (1998).
[32] P. O. Jubert, O. Fruchart, and C. Meyer, Phys. Rev. B **64**, 115419 (2001).
[33] O. Fruchart, J.-C. Toussaint, P.-O. Jubert, W. Wernsdorfer, R. Hertel, J. Kirschner, and D. Mailly, Phys. Rev. B **70**, 172409 (2004).
[34] P. Müller and R. Kern, Surf. Sci. **457**, 229 (2000).
[35] J. Stöhr, B. D. Hermsmeier, M. G. Samant, G. R. Harp, S. Koranda, D. Dunham, and B. P. Tonner, Science **259**, 658 (1993).
[36] A. Locatelli, S. Cherifi, S. Heun, M. Marsi, K. Ono, A. Pavlovska, and E. Bauer, Surf. Rev. Lett. **9**, 171 (2002).
[37] A. Locatelli, A. Bianco, D. Cocco, S. Cherifi, S. Heun, M. Marsi, M. Pasqualetto, and E. Bauer, J. Phys. IV **104**, 99 (2003).
[38] R. Hertel, J. Appl. Phys. **90**, 5752 (2001).

[39] W. H. Press, B. P. Flannery, S. A. Teukolsky, and W. T. Vetterling, *Numerical Recipies: The art of scientific computing* (Cambridge University Press, Cambridge, UK, 1986).
[40] H. A. M. Van Den Berg, J. Appl. Phys. **60**, 1104 (1986).
[41] H. A. M. Van Den Berg and A. H. J. Van Den Brandt, J. Appl. Phys. **62**, 1952 (1987).
[42] W. Rave and A. Hubert, IEEE Trans. Magn. **36**, 3886 (2000).
[43] A. S. Arrott, B. Heinrich, and A. Aharoni, IEEE Trans. Magn. **15**, 1228 (1979).
[44] A. S. Arrott and J.-G. Lee, J. Appl. Phys. **79**, 5752 (1979).
[45] L. Landau and E. M. Lifshitz, Phys. Z. Sowjetunion **8**, 153 (1935).
[46] S. Tsukahara and H. Kawakatsu, J. Phys. Soc. Jpn. **32**, 72 (1972).
[47] M. J. Donahue, J. Appl. Phys. **83**, 6491 (1998).
[48] R. Hertel and H. Kronmüller, IEEE Trans. Magn. **34**, 3922 (1998).
[49] A. E. LaBonte, J. Appl. Phys. **40**, 2450 (1969).
[50] A. S. Arrott and T. L. Templeton, Physica B **233**, 259 (1997).
[51] R. Hertel and H. Kronmüller, J. Appl. Phys. **85**, 6190 (1999).
[52] M. Bode, A. Wachowiak, J. Wiebe, A. Kubetzka, M. Morgenstern, and R. Wiesendanger, Appl. Phys. Lett. **84**, 948 (2004).
[53] C. G. Harrison and K. D. Leaver, Phys. Status Solidi A **15**, 415 (1973).
[54] The numerous images of magnetic domains in the famous textbook by Hubert and Schäfer (Ref. 5) may give the reader an impression of the beauty of magnetic domain patterns.
[55] http://www.elettra.trieste.it/nanospectroscopy/userarea/dataanalysis.html.
[56] Note that the Q factor is originally defined for crystals of *uniaxial* magnetocrystalline anisotropy. A comparison between the maximum stray field energy and the maximum uniaxial anisotropy energy leads to the argument used here for $Q \ll 1$. In the present case of cubic anisotropy, the quantitative interpretation Q of is less rigorous, but we can still assume that a value $Q \ll 1$ corresponds to a magnetically soft material.
[57] By flipping the magnetization $\boldsymbol{M} \rightarrow -\boldsymbol{M}$, four further domain structures can be obtained which correspond to a set of magnetization states with opposite chirality of the central vortex. Owing to time-inversion symmetry, the energy of these structures is identical to the ones prior to the inversion of $\boldsymbol{M}$, and their topology is obviously the same, too. It is therefore sufficient to consider only one type of vortex chirality.
[58] R. Hertel (unpublished).
[59] Similarly, Aharoni stated in his textbook (Ref. 7, p.173): "With present computers it is not even possible to find the lowest-energy configuration of a single wall, (…) let alone (…) any (…) true three-dimensional magnetization distribution."